



# A new multi-threshold image segmentation approach using state transition algorithm



Jie Han, Chunhua Yang, Xiaojun Zhou\*, Weihua Gui

School of Information Science and Engineering, Central South University, Changsha 410083, PR China

## ARTICLE INFO

### Article history:

Received 21 July 2015  
Revised 24 January 2017  
Accepted 9 February 2017  
Available online 22 February 2017

### Keywords:

Image segmentation  
State transition algorithm  
Multilevel thresholding  
Global optimization

## ABSTRACT

Thresholding plays an important role in image segmentation and image analysis. In this paper, the normalized histogram of an image is fitted by a linear combined normal distribution functions and each normal distribution function represents a class of pixels, whereas the parameters like the mean, the variance and the weights in the fitting function are undetermined. By transforming the fitting problem into a nonlinear and non-convex optimization problem, the state transition algorithm (STA) which is a new global optimization method is used to choose the optimal parameters of the fitting function. The effectiveness of proposed approach in multilevel thresholding problems is tested by several experimental results. By comparing with OTSU, particle swarm optimization (PSO), genetic algorithm (GA) and differential evolution (DE) algorithm, it has shown that STA has competitive performance in terms of both optimization results and thresholding segmentation.

© 2017 Elsevier Inc. All rights reserved.

## 1. Introduction

The process of image segmentation can subdivide a digital image into several regions according to the requirement of the problem to be solved. The segmentation result of an image determines the eventual success of analysis for computerized procedures [1]. With proper segmentation, an image can be described simply by means of meaningful things which are easier to analyze. In general, the intensity values assigned to the same region are substantially similar, and the intensity values from the adjacent regions are significantly different. In all possible approaches of image segmentation, thresholding plays an important role in practical applications. It can be applied to many areas such as document image analysis [2,3], image enhancement [4,5], feature extraction, map analysis [6], industrial inspection, and medical image processing.

Commonly, there are two major types of thresholding segmentation problems: single thresholding and multiple thresholding. For single thresholding, there is only one threshold, which means the entire image can be divided into two classes: the background and the foreground. Whereas for multiple thresholding segmentation, the distinct objects are subdivided from an image by multiple thresholds, and each thresholds should be appropriate for the corresponding segmentation [7].

Thresholding segmentation approach has attracted the attention of many researchers for several years, and various thresholding techniques have been investigated, consisting of parametric techniques and non-parametric techniques [8]. Parametric techniques begin with the assumption that the probability density function of each part of original image has a normal distribution. Then the normal distribution functions can be combined to fit the normalized histogram of the image

\* Corresponding author.

E-mail addresses: [hanjie@csu.edu.cn](mailto:hanjie@csu.edu.cn) (J. Han), [yqh@csu.edu.cn](mailto:yqh@csu.edu.cn) (C. Yang), [tiezhongyu2005@126.com](mailto:tiezhongyu2005@126.com), [michael.x.zhou@csu.edu.cn](mailto:michael.x.zhou@csu.edu.cn) (X. Zhou), [gwh@csu.edu.cn](mailto:gwh@csu.edu.cn) (W. Gui).

and the relevant parameters of such a fitting are estimated [9–12]. On the other hand, non-parametric techniques, including entropy [13], error minimization [14], and between-class variance [15], use some dividing criteria to compute the threshold values. The difference between parametric and non-parametric techniques lies in the criteria for threshold selection. The non-parametric techniques are more efficient and simpler [16], but they may cost too much computation time especially when dealing with multi-threshold image segmentation problems.

Optimization approaches in recent years have been used to solve multilevel thresholding segmentation problems. The estimation of parameters in the fitting problem can be transformed into an optimization problem. Since parametric techniques use transcendental functions, such as exponential function, the parameter estimation problem is usually a nonlinear and non-convex optimization problem. Hence, it may not only have multiple disconnected feasible regions but also multiple locally optimal points in such optimization problem. This problem is intrinsically very difficult to solve and the time required to solve this problem increases rapidly with the number of variables and constraints. There are a variety of methods for solving this problem, and stochastic global optimization algorithms are the most popular and effective type of methods [17–19].

Stochastic global optimization algorithms, such as genetic algorithms and evolutionary algorithms, maintain a population of candidate solutions, increasing the probability of finding the global optimum [20]. Based on the theory of state and state transition, a novel stochastic global optimization method named state transition algorithm (STA) has been proposed in [21–25], which have strong ability of both global search and local search by using four special state transformation operators, i.e., rotation, translation, expansion and axesion. The superiority of the STA has been testified by comparing with other global optimization algorithms such as genetic algorithm (GA) [26], particle swarm optimization (PSO) [27] and differential evolution (DE) [28] algorithm. Thus, a multi-threshold image segmentation approach using STA is investigated [29]. Based on the preliminary work of this study, the detailed process of multi-thresholding segmentation by using state transition algorithm is illustrated in this paper. Moreover, the image denoising process is introduced to obtain better segmentation results and the performance of the STA is compared with more optimization algorithms in terms of both computational cost and solution precision. In addition, we add three test images, including medical images and human image, to verify the effectiveness of proposed method.

The remainder of this paper is organized as follows. Section 2 provides the optimization problem by using a combined normal distribution functions to fit the normalized histogram of the image. Section 3 introduces the state transition algorithm and the whole process of multi-threshold segmentation is presented in Section 4. Section 5 demonstrates the effectiveness of proposed method by experimental results. Finally, the main conclusions of this paper is drawn in Section 6.

## 2. Normal distribution fitting

The image histogram with  $L$  total possible intensity levels in the range  $[0, L - 1]$  is defined as the following discrete function:

$$h(r_j) = n_j, \tag{1}$$

where  $n_j$  represents the number of pixels in the image and its intensity level is  $r_j$ . In general, for convenience of analysis, all elements of  $h(r_j)$  in the image will be divided by the total number of pixels  $n$  to obtain the normalized histogram

$$p(r_j) = \frac{h(r_j)}{n} = \frac{n_j}{n}, \quad \forall j = 0, 1, \dots, L - 1, \tag{2}$$

where  $p(r_j)$  is an estimation of the probability of occurrence of intensity level  $r_j$  in an image. The sum of all components of normalized histogram is equal to 1. In order to fit the normalized histogram, the following form of a linear combined normal distribution functions is used:

$$p^* = \sum_{i=1}^K \rho_i \cdot p_i^*(x) = \sum_{i=1}^K \frac{\rho_i}{\sqrt{2\pi}\sigma_i} \exp\left[-\frac{(x - \mu_i)^2}{2\sigma_i^2}\right]$$

$$\sum_{i=1}^K \rho_i = 1, \tag{3}$$

where  $K$  means the number of classes in the image,  $p_i^*(x)$  represents the  $i$ th normal distribution function,  $\rho_i$  is the weight of class  $i$ , the mean and the variance of the  $i$ th part are denoted by  $\mu_i$  and  $\sigma_i^2$ , respectively. The fitting function needs to be consistent with the normalized histogram data, usually by the means of the least mean square error approach. Let define  $\Omega = \{\rho_i, \mu_i, \sigma_i; i = 1, 2, \dots, K\}$ , the optimization problem is constructed as follows [1]:

$$\min E(\rho_i, \mu_i, \sigma_i, \dots) = \frac{1}{L} \sum_{j=0}^{L-1} [p^*(x_j, \rho_i, \mu_i, \sigma_i, \dots) - p(x_j)]^2$$

$$\text{s.t. } \sum_{i=1}^K \rho_i = 1, \tag{4}$$

where  $E$  means the objective function,  $p^*(\cdot)$  denotes the fitting function,  $p(\cdot)$  is the probability of occurrence, and  $x_j$  represents the  $j$ th intensity level in the range  $[0, L - 1]$ . By using the penalty method to dealing with the constraints, the problem (4) can be reformulated as follows [29]:

$$\min E(\rho_i, \mu_i, \sigma_i, \dots) = \frac{1}{L} \sum_{j=1}^{L-1} [p^*(x_j, \rho_i, \mu_i, \sigma_i, \dots) - p(x_j)]^2 + \omega \left[ \left( \sum_{i=1}^K \rho_i \right) - 1 \right]^2, \quad (5)$$

where  $\omega$  is the penalty factor.

This optimization problem is nonlinear and non-convex due to the presence of the term  $\exp(\cdot)$  in  $p^*(\cdot)$ . Because of the non-convexity of this problem, it has multiple locally optimal points. Therefore, the state transition algorithm which is a stochastic global optimization algorithm is adopted to find the global optimum in this study.

### 3. State transition algorithm

Based on the control theory of state transition and state space representation, a novel stochastic global optimization method called state transition algorithm (STA) has been proposed recently, in which, the state represents an optimization problem's solution, and the state transition means the process of updating the current solution [21]. In general, the unified form of generation of solution in STA can be described as follows:

$$\begin{cases} \mathbf{x}_{k+1} = A_k \mathbf{x}_k + B_k \mathbf{u}_k \\ y_{k+1} = f(\mathbf{x}_{k+1}), \end{cases} \quad (6)$$

where  $\mathbf{x}_k \in \mathbb{R}^n$  means a state, which corresponds to the optimization problem's solution;  $A_k$  and  $B_k$  are state transition matrices which has proper dimensions;  $\mathbf{u}_k$  is a function of  $\mathbf{x}_k$  as well as history states;  $f$  represents the evaluation function or objective function.

There are four special operators of state transformation designed by referring to multifarious types of space transformations.

#### 1. Rotation transformation

$$\mathbf{x}_{k+1} = \mathbf{x}_k + \alpha \frac{1}{n \|\mathbf{x}_k\|_2} R_r \mathbf{x}_k, \quad (7)$$

where  $\alpha$  is the rotation factor which is a positive constant;  $R_r \in \mathbb{R}^{n \times n}$  means a random matrix whose elements within the range of  $[-1, 1]$ .

#### 2. Translation transformation

$$\mathbf{x}_{k+1} = \mathbf{x}_k + \beta R_t \frac{\mathbf{x}_k - \mathbf{x}_{k-1}}{\|\mathbf{x}_k - \mathbf{x}_{k-1}\|_2}, \quad (8)$$

where  $\beta$  is the translation factor which is a positive constant;  $R_t \in \mathbb{R}$  means a random variable whose elements within the range of  $[0, 1]$ .

#### 3. Expansion transformation

$$\mathbf{x}_{k+1} = \mathbf{x}_k + \gamma R_e \mathbf{x}_k, \quad (9)$$

where  $\gamma$  is the expansion factor which is a positive constant;  $R_e \in \mathbb{R}^{n \times n}$  means a random diagonal matrix whose elements subjecting to the Gaussian distribution.

#### 4. Axesion transformation

$$\mathbf{x}_{k+1} = \mathbf{x}_k + \delta R_a \mathbf{x}_k, \quad (10)$$

where  $\delta$  is the axesion factor which is a positive constant;  $R_a \in \mathbb{R}^{n \times n}$  means a random diagonal matrix whose elements subjecting to the Gaussian distribution and there are only one random position with a nonzero value.

The following pseudocodes outline the procedure of the basic state transition algorithm.

- 1: **repeat**
- 2:   **if**  $\alpha < \alpha_{\min}$  **then**
- 3:      $\alpha \leftarrow \alpha_{\max}$
- 4:   **end if**
- 5:   Best  $\leftarrow$  expansion(funcn, Best, SE,  $\beta$ ,  $\gamma$ )
- 6:   Best  $\leftarrow$  rotation(funcn, Best, SE,  $\alpha$ ,  $\beta$ )
- 7:   Best  $\leftarrow$  axesion(funcn, Best, SE,  $\beta$ ,  $\delta$ )
- 8:    $\alpha \leftarrow \frac{\alpha}{f_c}$
- 9: **until** the specified termination criterion is met

where  $SE$  is the search enforcement, which indicates the number of times by a certain operator to transform, and a new optimal solution is selected by using the “greedy criterion”. Besides, the translation transformation is only performed when other transformation operators find a better solution.

In STA, the rotation transformation operator has the ability of local search, and the rotation factor  $\alpha$  can adjust the search range by exponentially reducing from a maximum value  $\alpha_{\max}$  to a minimum value  $\alpha_{\min}$ . The translation transformation has the function of line search. The expansion transformation is designed for global search, which can search the entire space with probability, and the axesion transformation is used to strengthen the ability of single dimensional search as well as global search.

#### 4. Multi-threshold image segmentation approach

##### 4.1. Thresholding value calculation

After using STA to fit the normalized histogram of original image, the optimal thresholding values can be calculated by minimizing the overall probability error, which is given by

$$\min E(T_i) = \rho_{i+1} \cdot E_1(T_i) + \rho_i \cdot E_2(T_i), \quad (11)$$

$$i = 1, 2, \dots, K - 1,$$

where  $T_i$  is the thresholding level between the  $i$ th and the  $(i + 1)$ th parts. In this function, the detailed form is

$$E_1(T_i) = \int_{-\infty}^{T_i} p_{i+1}^*(\mathbf{x}) d\mathbf{x} \quad (12)$$

and

$$E_2(T_i) = \int_{T_i}^{\infty} p_i^*(\mathbf{x}) d\mathbf{x}. \quad (13)$$

$E_1(T_i)$  is the probability of classifying the pixels in the  $(i + 1)$ th part to the  $i$ th part by mistake, and  $E_2(T_i)$  is the probability of erroneously categorizing the pixels in the  $i$ th part to the  $(i + 1)$ th part. When the error  $E(T_i)$  is minimized, the  $T_i$  will be obtained. Based on the knowledge of calculus, by differentiating  $E(T_i)$  with respect to  $T_i$ , we have

$$\begin{aligned} \frac{dE(T_i)}{dT_i} &= 0 \\ \Leftrightarrow \rho_{i+1} \frac{dE_1(T_i)}{dT_i} + \rho_i \frac{dE_2(T_i)}{dT_i} &= 0 \\ \Leftrightarrow \rho_{i+1} p_{i+1}^*(T_i) - \rho_i p_i^*(T_i) &= 0 \\ \Leftrightarrow \frac{\rho_{i+1}}{\sqrt{2\pi}\sigma_{i+1}} \exp\left[-\frac{(T_i - \mu_{i+1})^2}{2\sigma_{i+1}^2}\right] - \frac{\rho_i}{\sqrt{2\pi}\sigma_i} \exp\left[-\frac{(T_i - \mu_i)^2}{2\sigma_i^2}\right] &= 0 \\ \Leftrightarrow \frac{\exp\left[-\frac{(T_i - \mu_{i+1})^2}{2\sigma_{i+1}^2}\right]}{\exp\left[-\frac{(T_i - \mu_i)^2}{2\sigma_i^2}\right]} &= \frac{\rho_i \sigma_{i+1}}{\rho_{i+1} \sigma_i} \\ \Leftrightarrow \frac{(T_i - \mu_i)^2}{2\sigma_i^2} - \frac{(T_i - \mu_{i+1})^2}{2\sigma_{i+1}^2} &= \ln \frac{\rho_i \sigma_{i+1}}{\rho_{i+1} \sigma_i} \\ \Leftrightarrow (\sigma_i^2 - \sigma_{i+1}^2) T_i^2 + [2(\mu_i \sigma_{i+1}^2 - \mu_{i+1} \sigma_i^2)] T_i + & \\ + (\sigma_i \mu_{i+1})^2 - (\sigma_{i+1} \mu_i)^2 + 2(\sigma_i \sigma_{i+1})^2 \ln\left(\frac{\sigma_{i+1} \rho_i}{\sigma_i \rho_{i+1}}\right) &= 0. \end{aligned} \quad (14)$$

Therefore, the following equations can be used to obtain the optimum threshold level  $T_i$  [29]:

$$AT_i^2 + BT_i + C = 0, \quad (15)$$

where,

$$\begin{aligned} A &= \sigma_i^2 - \sigma_{i+1}^2, \\ B &= 2(\mu_i \sigma_{i+1}^2 - \mu_{i+1} \sigma_i^2), \\ C &= (\sigma_i \mu_{i+1})^2 - (\sigma_{i+1} \mu_i)^2 + 2(\sigma_i \sigma_{i+1})^2 \ln\left(\frac{\sigma_{i+1} \rho_i}{\sigma_i \rho_{i+1}}\right). \end{aligned} \quad (16)$$

Although the above quadratic equation has two possible solutions, only the positive one which within the interval is chosen for segmentation [28,30].

#### 4.2. Image segmentation and denoising

It is known that an image can be defined as a two-dimensional function,  $f(x, y)$ , where  $x$  and  $y$  are spatial coordinates, and the amplitude of  $f$  at any coordinate pair  $(x, y)$  is the intensity level of the image at that point. Based on the threshold values  $T = \{T_1, T_2, \dots, T_{K-1}\}$ ,  $T_1 < T_2 < \dots < T_{K-1}$ , an original image can be separated into  $K$  classes. For example, an image can be segmented into three classes by two thresholding values as follows:

$$\begin{cases} \Phi_1 & \text{if } f(x, y) \leq T_1 \\ \Phi_2 & \text{if } T_1 < f(x, y) \leq T_2 \\ \Phi_3 & \text{if } f(x, y) > T_2. \end{cases} \quad (17)$$

where  $\Phi_1$ ,  $\Phi_2$  and  $\Phi_3$  represent three different classes, respectively,  $T_1$  and  $T_2$  denote the threshold values.

Considering that there may exist noise in the image, next, an image denoising algorithm is introduced. Firstly, each class of the segmented image is converted into a binary image. Specifically, when dealing with the class  $\Phi_1$ , every point  $(x, y)$  in this class can be regarded as the foreground point of the first class; otherwise, the point is called a background point. In other words, the binary image of the class  $\Phi_1$  is given by

$$g_1(x, y) = \begin{cases} 1 & \text{if } (x, y) \in \Phi_1 \\ 0 & \text{otherwise.} \end{cases} \quad (18)$$

In this way, the class  $\Phi_1$  is transformed into a binary image and the process of image denoising can be implemented. In order to remove noisy objects from the segmented image, the operator “bwareaopen” is used for image post-processing.

As a morphological operator, the “bwareaopen” can delete connected components that are smaller than a predefined threshold [31]. It is also a predefined operator in MATLAB, with two parameters to adjust: the connectivity and the maximal size of pixels to remove [32]. In this paper, the connectivity is set at 8. As a result, the objects in foreground that have fewer than 64 pixels and the objects in background that have fewer than 256 pixels are removed from the binary image. After the denoising process for each class of the binary image, the final thresholding results can be obtained as follows:

$$g(x, y) = \begin{cases} a & \text{if } g_1(x, y) = 1 \\ b & \text{if } g_2(x, y) = 1 \\ c & \text{if } g_3(x, y) = 1, \end{cases} \quad (19)$$

where  $g(x, y)$  is the final segmented image,  $a$ ,  $b$  and  $c$  are three distinct intensity values,  $g_1$ ,  $g_2$  and  $g_3$  are the denoising results of the corresponding classes.

#### 4.3. Flow chart of the proposed approach

The flow chart of multi-threshold segmentation using state transition algorithm is shown in Fig. 1. First and foremost, it should determine the type of the original image, and if its type is RGB, the operator “rgb2gray” is executed. Then, based on the normalized histogram, a fitting problem is constructed and its optimal parameters are estimated by using STA. According to the Eqs. (15) and (16), the threshold values can be computed, and after image segmentation, a denoising process is carried out. In the end the final segmented result is outputted.

### 5. Computational results and analysis

In this section, several experiments are carried out to evaluate the performance of the proposed approach. Most of the test images are from the segmentation evaluation database [33] and USC-SIPI image database, which have been transformed into gray-scale images. In order to compare the segmentation results with other references, one medical image from Human Connectome Project Wu-Minn Consortium is chosen for analysis. In the same time, the performance of the OTSU method, genetic algorithm (GA), particle swarm optimization algorithm (PSO) and differential evolution (DE) algorithm in MATLAB are investigated for comparison. Fig. 2 shows the detailed information of all test images, including the original images, original normalized histograms, the maximum and minimum values of intensity levels.

#### 5.1. Parameters setting

The tests in this paper are all run under the software platform of MATLAB(Version R2010b). For STA, we use the same parameter settings as in previous papers [21,22,34,35] which all successfully dealt with the optimization problems such as benchmark, nonlinear system control and resolution of overlapping linear sweep voltammetric peaks, and the parameter settings in these papers can be considered as the empirical values which are also appropriate for the problems in this paper. The details of parameter settings of STA are shown in Table 1.

For fairness, we also adjust the parameter settings in other algorithms to obtain plausible solutions. As for GA, after combining the existing parameter settings in [26], the final parameters of GA in this paper are set as follows: the crossover rate  $P_c$  equals to 0.95, the mutation rate  $P_m$  equals to 0.1, the crossover index  $\eta_c$  equals to 5 and the mutation index  $\eta_m$  equals to 20. Then, for PSO, based on the previous setting in [27], the measurements in this paper is set to 6 and this

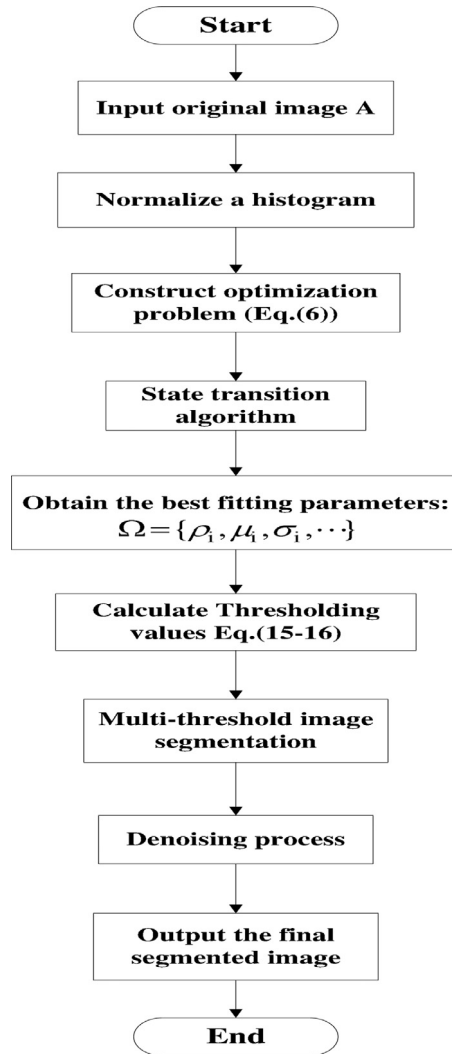


Fig. 1. Flow chart of multi-threshold image segmentation using STA.

Table 1  
Parameter settings of STA.

Parameter	Value
SE	30
$\alpha$	$1 \rightarrow 1e-4$
$\beta$	1
$\gamma$	1
$\delta$	1
fc	2

parameter can influence the cooperation performance between multiple Monte Carlo measurements for each particle. As for DE, we use the MATLAB codes provided by the author in [28] with minor revisions for this experiment to obtain proper results. The details of parameter are set as follows: the scaling factor  $F$  is approximated by a normal distribution with mean value 0.5 and standard deviation 0.3, denoted by  $N(0.5, 0.3)$ , and the crossover rate  $CR$  equals to 0.5.

In the experiments, the empirical value of population size is 30, and in order to determine the number of iterations, the iterative results are analyzed. For example, Fig. 3 shows the fitness values with respect to the number of iterations for the building image with two threshold, and we can find that the iterative curves of STA, GA, PSO and DE nearly have no update from 90, 85, 70 and 75 generations, respectively. It is almost unnecessary to increase the number of iterations, so the the maximum number of iterations is chosen 100. For the parameters in handling constraints, the penalty factor  $\omega$  is chosen 1 based on empirical tests.




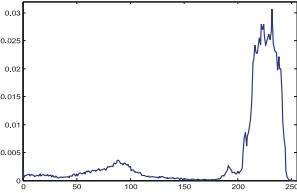
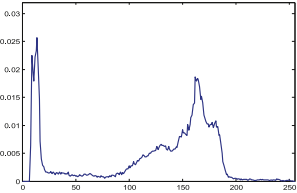
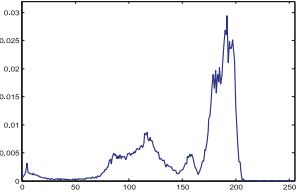

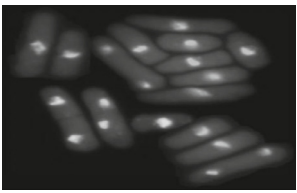
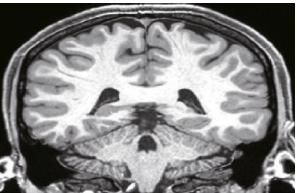
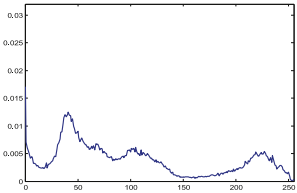
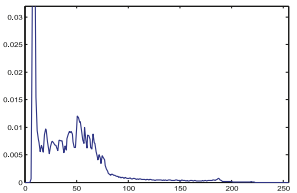
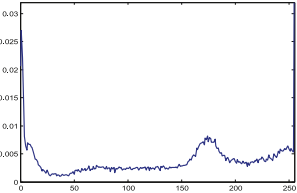
Name	Building	Camerman	Ship
Original images			
Original histogram			
Intensity level	[0, 252]	[7, 253]	[0,255]
Name	Flower	Cell	Medical
Original images			
Original histogram			
Intensity level	[0, 255]	[6, 222]	[0,255]

Fig. 2. The detailed information of all test images.

## 5.2. Experimental results

The goal of these experiments is to divide the image into several different categories and segment the objects from the background. The number of thresholds depends on the goal of segmentation, which means it can be determined by the number of objects to be segmented. For example, according to the intensity levels of cell image, if the goal is to segment the cell from background, the number of thresholds is chosen at one, while if the goal is to separate the cell nucleus and cytoplasm from background, the tri-level thresholding is adopted. After image segmentation, a denoising algorithm is used to remove small connected components. The results are evaluated in two aspects: (1) the accuracy of the object to be segmented; (2) the speed of the algorithm and the precision of the solution.

Table 2 shows a Wilcoxon rank sum test [36,37] to analyze the performance of four different optimization algorithms. For each problem, 25 independent runs are performed and statistical results are provided including the mean and the standard deviation values. The last three rows of Table 2 summarize the experimental results.

Table 2 shows that STA is superior to PSO with high quality final solution with lower mean values and the performance of STA has competitive results when comparing with GA and DE since it has better solutions on more than half of cases. From the Wilcoxon rank sum test results, it is obvious that STA is superior to PSO in all cases and as for GA, there are 6 test results indicating that STA has better performance, and in other 6 tests they have same performance. Moreover, compared with EA, STA has better performance in 9 test and has similar performance in 3 tests. Thus, STA is almost either better or equal to other methods.



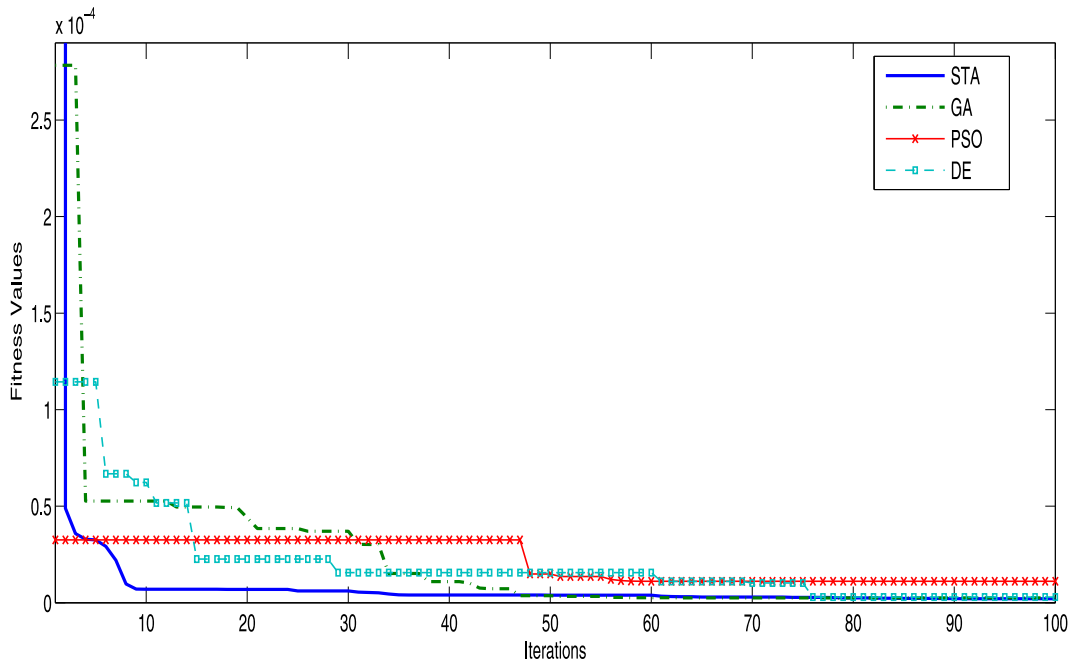


Fig. 3. The iterative curve of building image with two threshold.

Table 2

Wilcoxon rank sum test at a 0.05 significance level.

Problem	Number of thresholds	GA	PSO	DE	STA
Building	One	3.9183e-06±1.1070e-06	1.2688e-05±7.8604e-06	3.2572e-06±7.6862e-07	3.0568e-06±2.3967e-06
	Two	4.1842e-06±1.7419e-06	1.7258e-05±9.0199e-06	5.6244e-06±2.4326e-06	3.6515e-06±3.0098e-06
Camera	Two	9.4577e-06±4.8318e-06	1.6070e-05±2.0063e-06	1.3854e-05±8.8294e-07	7.3286e-06±7.6085e-06
	Four	1.3116e-05±3.4377e-06	1.7372e-05±2.4330e-06	1.1410e-05±2.7983e-06	3.7018e-06±2.5009e-06
Ship	Two	5.4406e-06±2.2723e-06	1.5144e-05±5.9656e-06	5.0947e-06±1.2986e-06	5.0943e-06±3.2859e-06
	Three	6.9180e-06±3.1320e-06	1.5758e-05±6.2529e-06	5.4512e-06±1.4634e-06	4.8615e-06±3.9356e-06
Flower	Two	3.1178e-06±4.4871e-07	4.6233e-06±5.7173e-07	3.7557e-06±3.0308e-07	2.9630e-06±9.4310e-07
	Three	3.2540e-06±4.7818e-07	4.4454e-06±7.4676e-07	3.3537e-06±3.7684e-07	2.9401e-06±1.2840e-06
Cell	One	2.7750e-05±3.9226e-05	2.4141e-04±4.2788e-05	1.4015e-04±6.0172e-05	2.6361e-05±3.6813e-05
	Two	1.7041e-05±9.3954e-06	2.3268e-04±6.5509e-05	1.4604e-04±6.9149e-05	1.1759e-05±2.3684e-05
Medical	Two	1.3623e-05±1.8519e-06	1.7059e-05±8.4868e-07	1.5710e-05±9.6495e-07	1.0787e-05±3.3281e-06
	Three	1.3079e-05±2.3304e-06	1.6555e-05±1.2119e-06	1.5381e-05±9.9667e-07	7.8375e-06±4.7180e-06
	-	6	12	9	
	+	0	0	0	
	≈	6	0	3	

“-”, “+”, and “≈” denote that the performance of the corresponding algorithm is worse than, better than, and similar to that of STA, respectively.

Table 3 shows the average execution time (in seconds) of optimization algorithms in each test using a 3.1 GHz Intel i5 PC with 2G RAM. In terms of the Table 3, we can find that the execution time increases with the number of thresholds. Moreover, the speed of STA is faster than GA, PSO and DE. For example, in the test of building image with two thresholds, the execution time of STA (1.2006 s) is less than the time of GA (1.2704 s), PSO (1.3721 s) and DE (1.2520), which indicates the high efficiency of STA.

Figs. 4–15 show the segmentation results of the test images. For each test, 25 independent runs are performed and the results of mode are chosen to represent the performance of these different approaches.

Figs. 4 and 5 summarize the thresholding results of the building image. Fig. 4(a)–(e) show the segmentation results of OTSU, STA, GA, PSO and DE with one threshold, respectively. The two buildings are all segmented from the background. But the results obtained by PSO erroneously classifies some pixels in the white part to the black part. Fig. 4(f)–(i) are the fitting curves obtained by STA, PSO, GA and DE. It is obvious that STA can fit the initial normalized histogram with lowest mean square error 2.4605e-006. The other three fitting results exist some distortions when fitting the original normalized histogram.

When the number of thresholds increases to two, the results from OTSU, STA, GA, PSO and DE are able to identify the objects better than the ones with lower thresholds, especially in the two buildings. It is obvious that STA and GA perform better than OTSU, PSO and DE according to Fig. 5(a)–(e). But the segmentation result obtained by GA is still imperfect. From



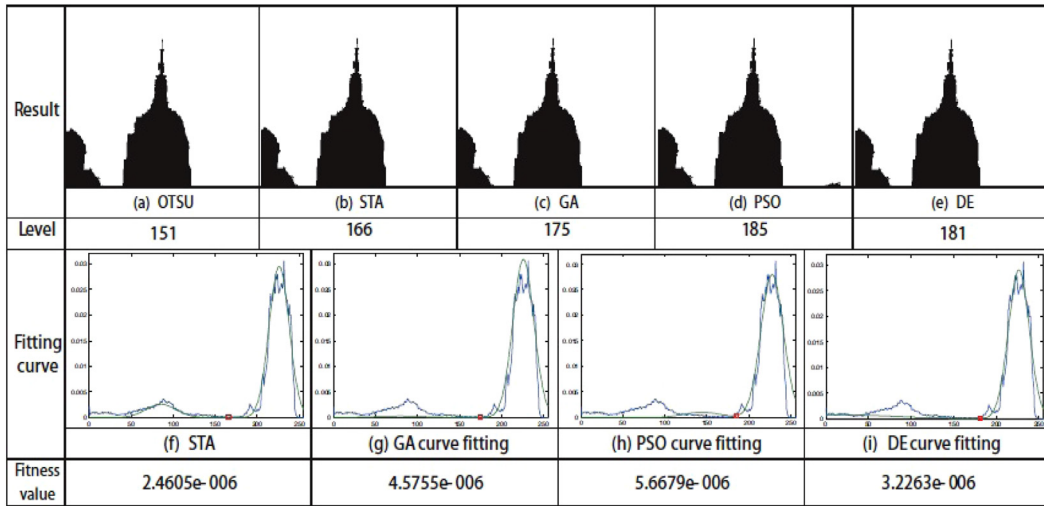


Fig. 4. Experimental results for building image with one threshold.

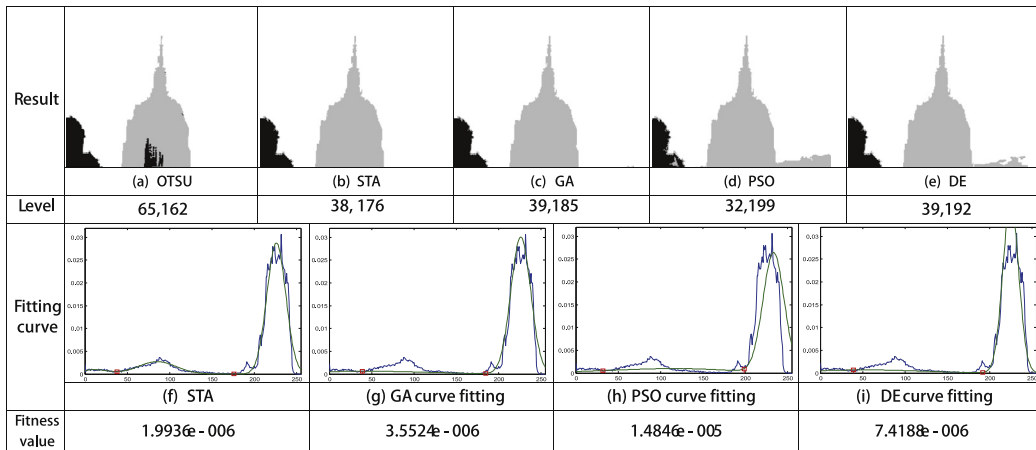


Fig. 5. Experimental results for building image with two thresholds.

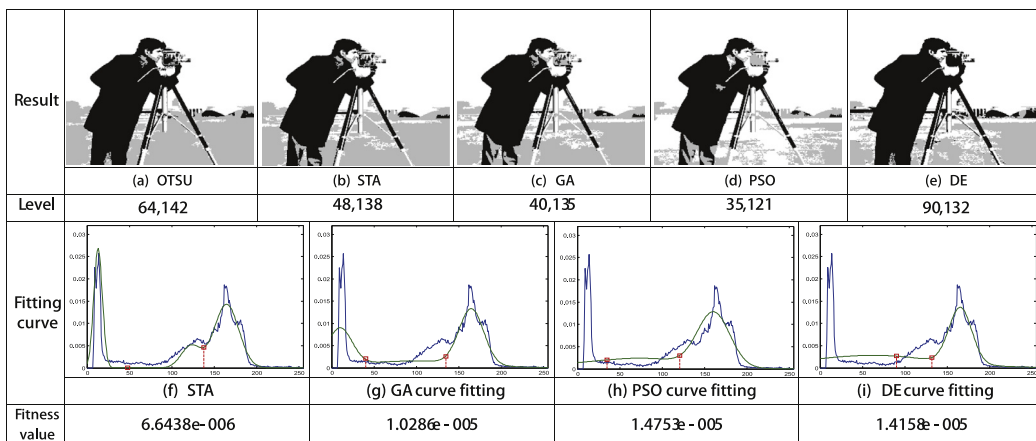


Fig. 6. Experimental results for cameraman image with two thresholds.

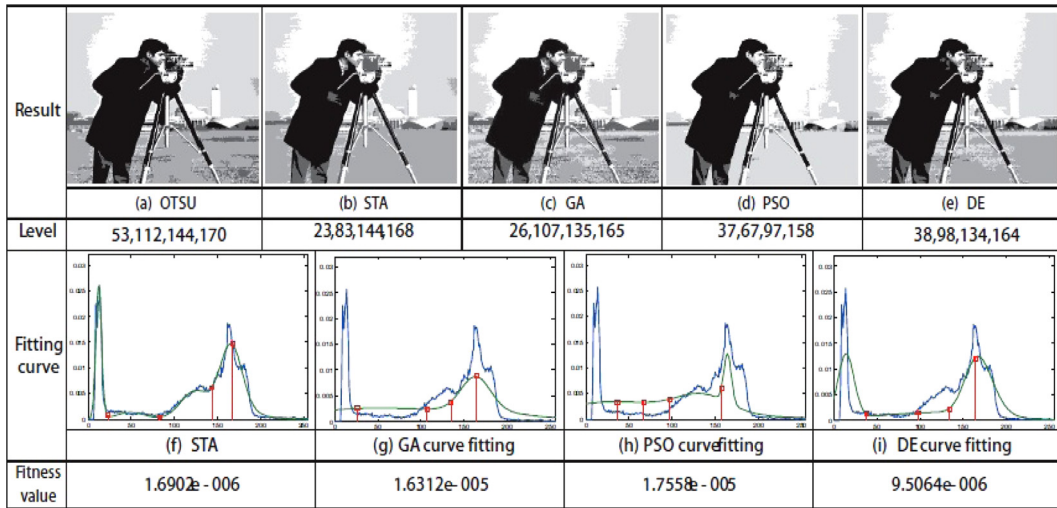


Fig. 7. Experimental results for cameraman image with four thresholds.

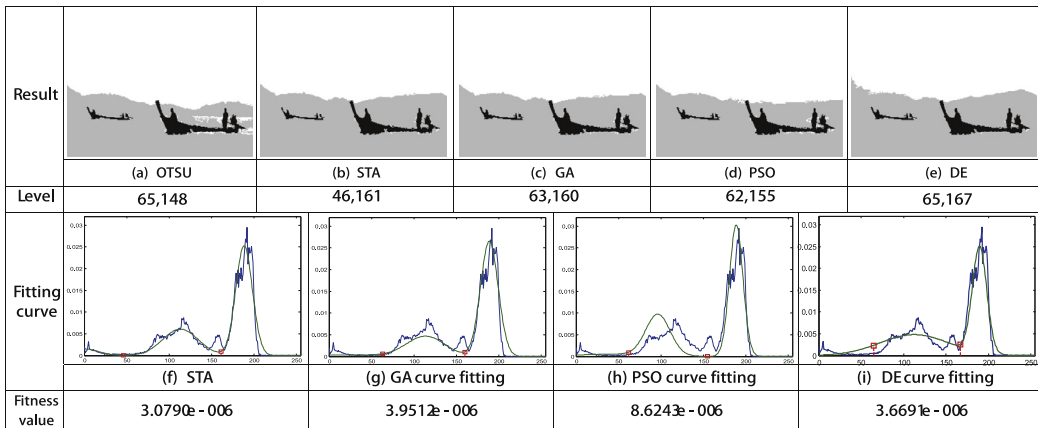


Fig. 8. Experimental results for ship image with two thresholds.

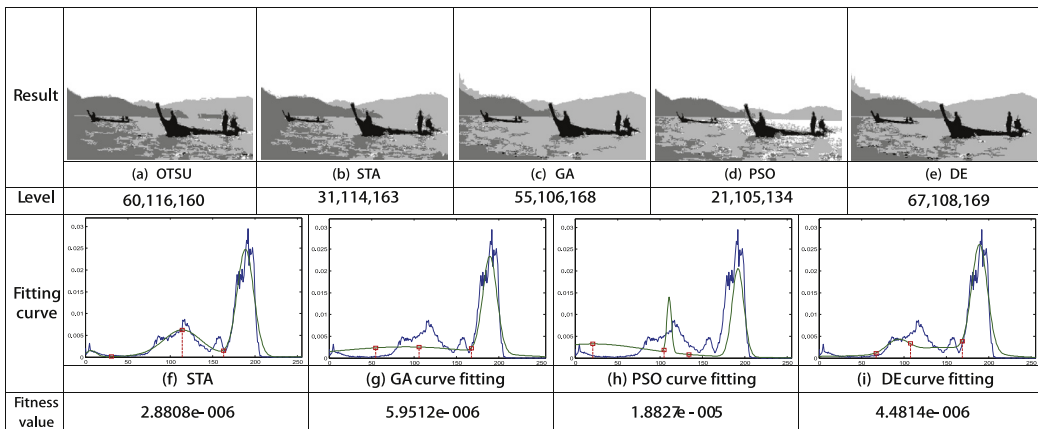


Fig. 9. Experimental results for ship image with three thresholds.

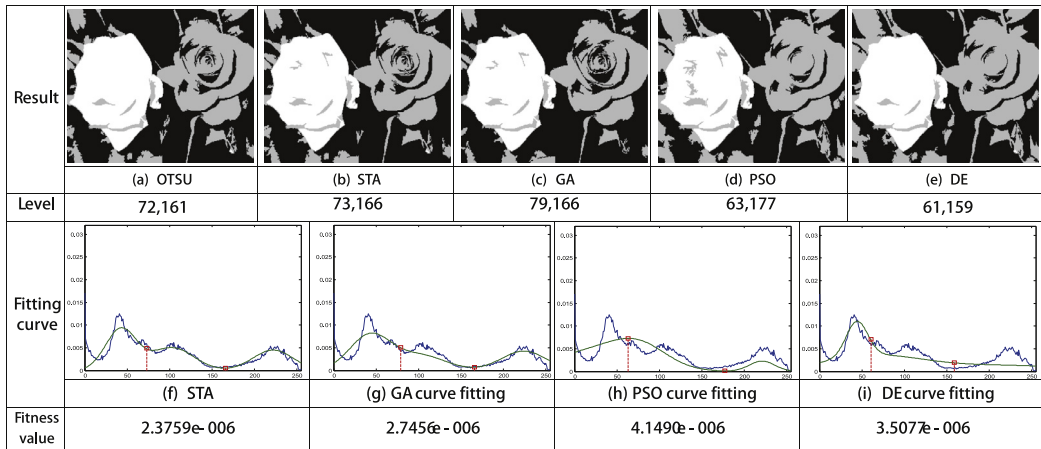


Fig. 10. Experimental results for flower image with two thresholds.

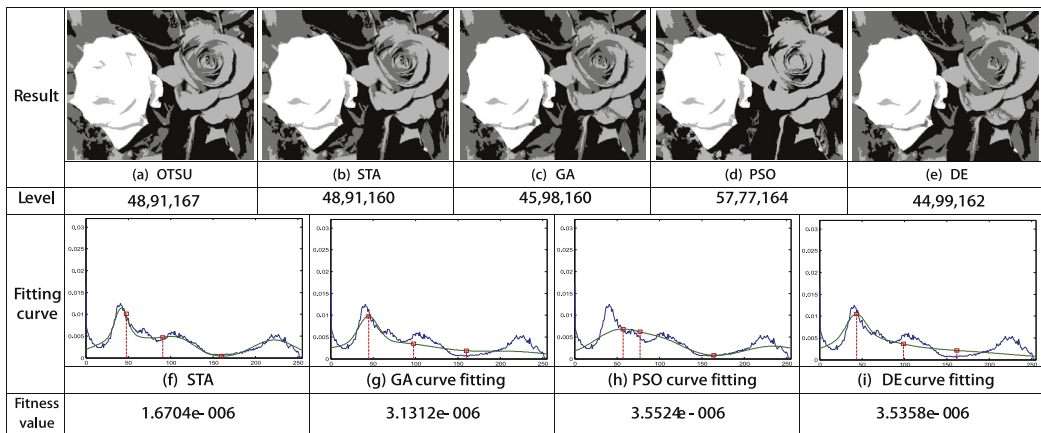


Fig. 11. Experimental results for flower image with three thresholds.

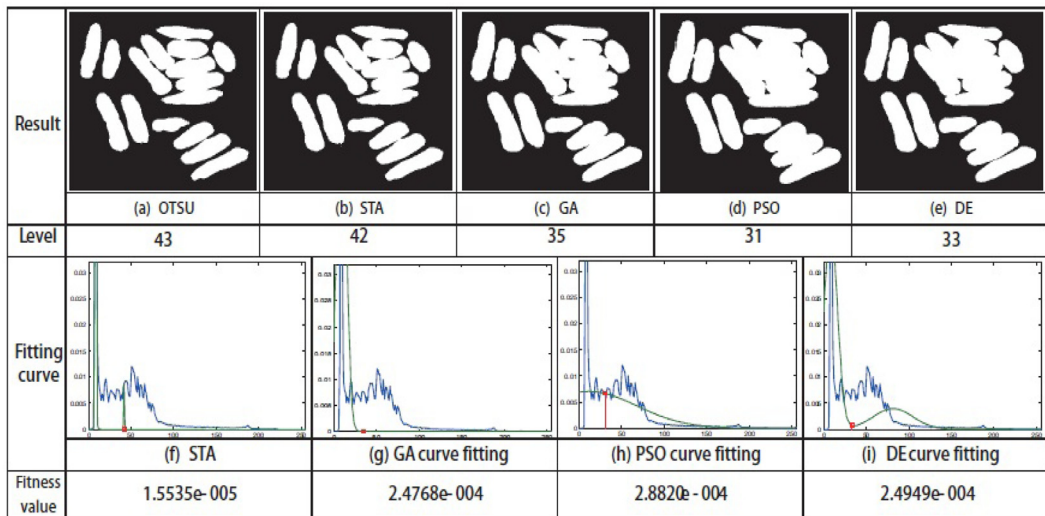
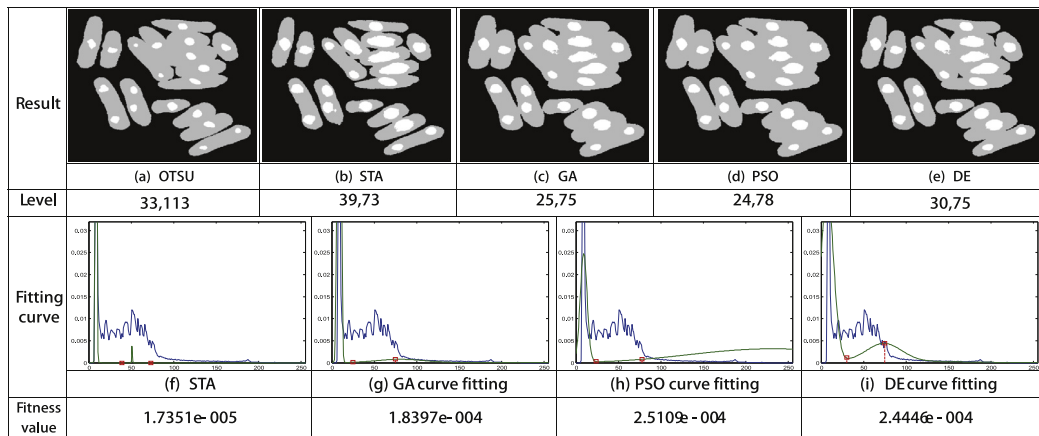


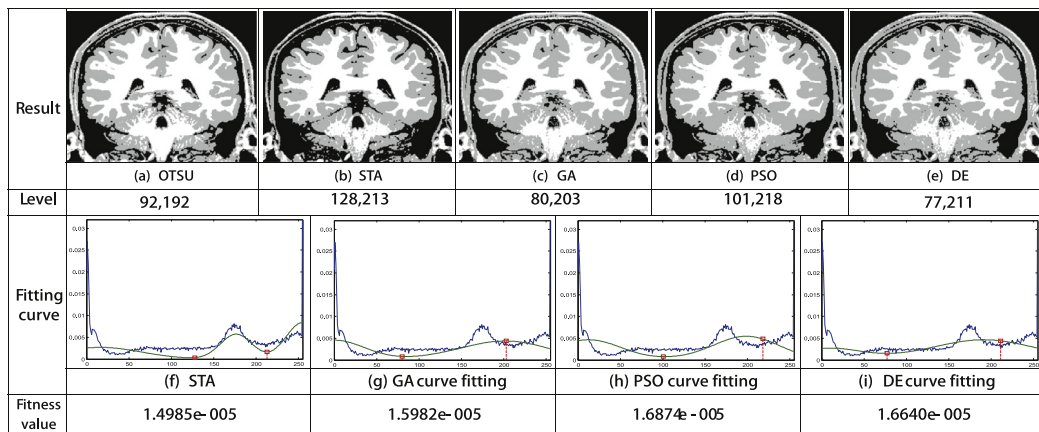
Fig. 12. Experimental results for cell image with one threshold.

**Table 3**  
The average execution time (s) of all test.

Problem	Number of thresholds	GA	PSO	DE	STA
Building	One	0.9401	1.0736	0.9671	0.9214
	Two	1.2704	1.3721	1.2520	1.2006
Cameraman	Two	1.2665	1.2584	1.2152	1.2138
	Four	2.0440	2.0617	1.9581	1.8294
Ship	Two	1.2699	1.3625	1.3651	1.2416
	Three	1.5788	1.7056	1.5983	1.5228
Flower	Two	1.2242	1.2388	1.2315	1.1596
	Three	1.5709	1.6390	1.6178	1.4373
Cell	One	0.8945	1.0506	0.9670	0.8532
	Two	1.2150	1.3500	1.2146	1.1960
Medical	One	1.0442	1.1637	1.0886	1.0301
	Two	1.5047	1.6686	1.7000	1.4671



**Fig. 13.** Experimental results for cell image with two thresholds.



**Fig. 14.** Experimental results for building image with one threshold.

Fig. 5(f), it is shown that the fitting curve obtained by the STA well fits the normalized histogram of the original image and its mean square error is  $1.9936e-006$ .

The segmentation results of cameraman image with two and four thresholds are shown in Figs. 6 and 7, correspondingly. Fig. 6(a)–(e) are the thresholding results obtained by OTSU, STA, GA, PSO and DE. For all results, the man is recognized by black part. The sky is mainly identified by white part except in Fig. 6(d) and the gray part in Fig. 6(d) is not performing as good as gray part in others. Fig. 6(f)–(i) show that the normalized histogram can be well fitted by STA and the mean square error of STA is very small which is only  $6.6438e-006$ .

In Fig. 7, there are five different colors in the segmentation results, including white, light gray, gray, dark gray and black. From Fig. 7(a)–(e), all of the results can identify the man with black and dark gray part. Fig. 7(a)–(c) and Fig. 7(e) can identify

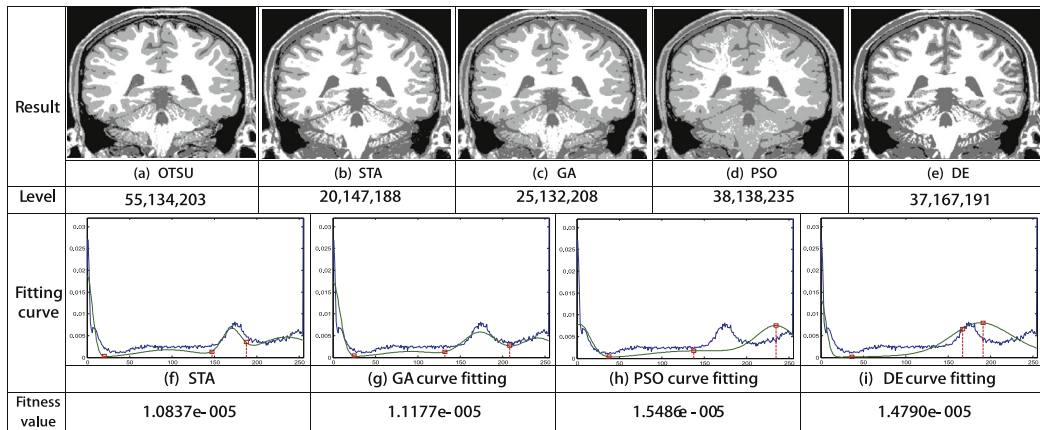


Fig. 15. Experimental results for building image with two thresholds.

the sky with white and light gray part, and the ground is described by gray part. But in Fig. 7(a), (c) and (e) obtained by OTSU, GA and DE, there are many interferences in the ground. Similar to Fig. 6, the fitted curve obtained by STA can also well approximate the normalized histogram with mean square error of  $1.6902e-006$ .

Figs. 8–9 are the results of ship image with two and three thresholds. Fig. 8(a)–(e) describe the segmentation results by OTSU, STA, GA, PSO and DE, respectively. All of the results can identify the ships with black part, the mountains and lakes with gray part, the sky with white part, but the gray part in Fig. 8(a) is still imperfect. Moreover, the gray part segmented by STA is more similar to the shape of the mountains. Fig. 8(f)–(i) illustrate that the fitting results of STA and GA are better than others with very small mean square error of  $3.0790e-006$  and  $3.9512e-006$ , respectively.

In order to identify two mountains, the thresholds are increased to three. According to Fig. 8(a)–(e), four-level segmentation does well in recognizing the two mountains but it creates some interferences in the surface of water. Fig. 8(c) and (e) has poor performance to identify the shape of mountains and the light gray part of Fig. 8(d) exist much more interferences than others. Fig. 8(f) shows that the STA can fit the normalized histogram accurately with the mean square error of  $2.8808e-006$ .

The segmentation results of flower image with two thresholds are shown in Fig. 10. OTSU, STA, GA, PSO and DE all perform similar according to the Fig. 10(a)–(e). Notice that, since the normalized histogram is a smooth curve, this image with low contrast is difficult to be segmented accurately. Compared with the original image in Fig. 2, the white part of Fig. 10(a)–(c) are closer to the left flower while the gray part of Fig. 10(d) and (e) are closer to the right flower. Fig. 10(f)–(i) show that the STA and GA have better fitting results which can approximate most peaks and valleys.

Fig. 11 is the four-level segmentation results of flower image. From Fig. 11(a)–(e), the OTSU, STA, GA and DE can identify the left flower with white part while PSO can identify the right flower with light gray part. Fig. 11(f)–(i) show that the STA, GA and DE can well fit the normalized histogram and their mean square error are only  $1.6704e-006$ ,  $3.1312e-006$  and  $3.5358e-006$ , respectively.

Figs. 12 and 13 are the bi-level and tri-level thresholding results of the cell image. The comparisons among those five different approaches show that all of results can identify the cell outlines but the segmentation results obtained by OTSU, STA and GA are more accurate and reasonable. The mean square error of STA is also showing better fitting results than others. Fig. 13 shows the segmentation result by two thresholds. Both OTSU and STA can identify the cell nucleus, but the gray part of Fig. 13(b) obtained by STA is more closer to the shapes of the cells. It means that the STA is more appropriate for solving the multi-threshold image segmentation problem of this kind of image. Fig. 13(f)–(i) show that the STA can fit the histogram with better results.

Figs. 14 and 15 summarize the thresholding results of the medical image. Fig. 14(a)–(e) show the segmentation results obtained by OTSU, STA, GA, PSO and DE, respectively. They all describe the white matter and cerebellum with white part, the gray matter with gray part, and the lacuna and paracele with black part. The differences among all results are not obvious to human eye and their fitting curves also with small distinction according to Fig. 14(f)–(i).

Fig. 15 is the four-level segmentation results of medical image. When the thresholds are increased to three, the lacuna can be segmented by black part and the paracele can be described by dark gray part according to Fig. 15(a)–(e). The results obtained by OTSU, STA and GA can identify the gray matter with gray part, while the results obtained by PSO can separate white matter with white part. Fig. 15(f)–(i) show that the fitting curves obtained by STA and GA well fit the initial normalized histogram and their mean square error are  $1.0837e-005$  and  $1.1177e-005$ , respectively.

## 6. Conclusion and future work

For a general image thresholding problem, a parametric technique associated with global optimization method is investigated in this paper. A linear combined normal distribution functions is used to fit the normalized histogram of an image,



and the fitting problem can be considered an optimization problem. Then the state transition algorithm which is a novel stochastic global optimization method is adopted to obtain the optimal parameters in the fitting function. Compared with OTSU, PSO, GA and DE, experimental results have shown that STA has competitive results in terms of both solution precision and image segmentation, which also testify the effectiveness of the proposed method. However, the main idea of this paper is based on the whole intensity information of the image, and future work may combine location information with thresholding method.

## Acknowledgments

The work was supported by the [National Natural Science Foundation of China](#) (Grant Nos. [61503416](#) and [61533021](#)), Key Exploration Project (Grant No. [7131253](#)), and the Foundation for Innovative Research Groups of the National Natural Science Foundation of China (Grant No. [61621062](#)).

## References

- [1] R.C. Gonzalez, R.E. Woods, *Digital Image Processing*, second ed., Prentice-Hall Inc., Upper Saddle River, NJ, 2002.
- [2] M., A. Zhao, Extraction of binary character/graphics images from grayscale document images, *Graph. Models Image Process.* 55 (3) (1993) 203–217.
- [3] T. Abak, U. Baris, B. Sankur, The performance of thresholding algorithms for optical character recognition, in: *Proceedings of the 4th International Conference on Document Analysis and Recognition*, Ulm, Germany, 1997, pp. 697–700.
- [4] J. Pan, C. Zhang, Q. Guo, Image enhancement based on the shearlet transform, *ICIC Exp. Lett.* 3 (3) (2009) 621–626.
- [5] Y. Zhang, C. Zhang, C. J. R. Zhang, An algorithm for enlarged image enhancement, *ICIC Exp. Lett.* 3 (3) (2009) 669–674.
- [6] O.D. Trier, A.K. Jain, Goal-directed evaluation of binarization methods, *IEEE Trans. Pattern Anal. Mach. Intell.* 17 (12) (1995) 1191–1201.
- [7] L. Chih-Chih, A novel image segmentation approach based on particle swarm optimization, *IEICE Trans. Fundam.* 89 (1) (2006) 324–327.
- [8] A.S. Abutaleb, Automatic thresholding of gray-level pictures using two-dimensional entropy, *Comput. Vis. Graph. Image Process.* 47 (1989) 22–32.
- [9] R.A. Fisher, The use of multiple measurements in taxonomic problems, *Ann. Eugen.* 7 (1936) 179–188.
- [10] D.M. Tsai, A fast thresholding selection procedure for multimodal and unimodal histograms, *Pattern Recognit. Lett.* 16 (1995) 653–666.
- [11] F. Yan, H. Zhang, C.R. Kube, A multistage adaptive thresholding method, *Pattern Recognit. Lett.* 26 (2005) 1183–1191.
- [12] A. Nakib, H. Oulhadj, P. Siarry, Image histogram thresholding based on multiobjective optimization, *Signal Process.* 87 (2007) 2516–2534.
- [13] J.N. Kapur, P.K. Sahoo, A.K.C. Wong, A new method for gray-level picture thresholding using the entropy of the histogram, *Comput. Vis. Graph. Image Process.* 29 (1985) 273–285.
- [14] J. Kittler, J. Illingworth, Minimum error thresholding, *Pattern Recognit.* 19 (1986) 41–47.
- [15] N. Otsu, A threshold selection method from gray-level histograms, *IEEE Trans. Syst. Man Cybern., SMC-B* (1979) 62–66.
- [16] A.K. Bhandari, V.K. Singh, A. Kumar, G.K. Singh, Cuckoo search algorithm and wind driven optimization based study of satellite image segmentation for multilevel thresholding using Kapur's entropy, *Expert Syst. Appl.* 41 (7) (2014) 3538–3560.
- [17] A. Baştürk, E. Günay, Efficient edge detection in digital images using a cellular neural network optimized by differential evolution algorithm, *Expert Syst. Appl.* 36 (8) (2009) 2645–2650.
- [18] P. Ghamisi, M.S. Couceiro, J.A. Benediktsson, N.M.F. Ferreira, An efficient method for segmentation of images based on fractional calculus and natural selection, *Expert Syst. Appl.* 39 (16) (2012) 12407–12417.
- [19] P. Huang, H. Cao, S. Luo, An artificial ant colonies approach to medical image segmentation, *Comput. Methods Programs Biomed.* 92 (3) (2008) 267–273.
- [20] H.V.H. Ayala, F.M.d. Santos, V.C. Mariani, L.d. S. Coelho, Image thresholding segmentation based on a novel beta differential evolution approach, *Expert Syst. Appl.* 42 (2015) 2136–2142.
- [21] X.J. Zhou, C.H. Yang, W.H. Gui, State transition algorithm, *J. Ind. Manag. Optim.* 8 (4) (2012) 1039–1056.
- [22] X.J. Zhou, C.H. Yang, W.H. Gui, Nonlinear system identification and control using state transition algorithm, *Appl. Math. Comput.* 226 (2014) 169–179.
- [23] X.J. Zhou, D.Y. Gao, C.H. Yang, W.H. Gui, Discrete state transition algorithm for unconstrained integer optimization problems, *Neurocomputing* 173 (2016) 864–874.
- [24] X.J. Zhou, D.Y. Gao, A.R. Simpson, Optimal design of water distribution networks by discrete state transition algorithm, *Eng. Optim.* 48 (4) (2016) 603–628.
- [25] F.X. Zhang, C.H. Yang, X.J. Zhou, W.H. Gui, Fractional-order PID controller tuning using continuous state transition algorithm, *Neural Comput. Appl.* (2016), doi:10.1007/s00521-016-2605-0.
- [26] S. Manikandan, K. Ramar, M.W. Iruthayarajan, K.G. Srinivasagan, Multilevel thresholding for segmentation of medical brain images using real coded genetic algorithm, *Measurement* 47 (2014) 558–568.
- [27] Y.Y. Li, L.C. Jiao, R.H. Shang, R. Stolkin, Dynamic-context cooperative quantum-behaved particle swarm optimization based on multilevel thresholding applied to medical image segmentation, *Inf. Sci.* 294 (2015) 408–422.
- [28] E. Cuevas, D. Zaldivar, M. PerezPerez-Cisneros, A novel multi-threshold segmentation approach based on differential evolution optimization, *Expert Syst. Appl.* 37 (7) (2010) 5265–5271.
- [29] J. Han, X.J. Zhou, C.H. Yang, W.H. Gui, A multi-threshold image segmentation approach using state transition algorithm, 2015, pp. 2662–2666.
- [30] V. Osuna-Enciso, E. Cuevas, H. Sossa, A comparison of nature inspired algorithms for multi-threshold image segmentation, *Expert Syst. Appl.* 40 (4) (2013) 1213–1219.
- [31] J.R. Nanduri, F.A. Pino-Romainville, I. Celik, CFD mesh generation for biological flows: geometry reconstruction using diagnostic images, *Comput. Fluids* 38 (2009) 1026–1032.
- [32] K.T. Morin, P.D. Carlson, R.T. Tranquillo, Automated image analysis programs for the quantification of microvascular network characteristics, *Methods* 84 (2015) 76–83.
- [33] S. Alpert, M. Galun, R. Basri, A. Brandt, Image segmentation by probabilistic bottom-up aggregation and cue integration, in: *Proceedings of the IEEE Conference on Computer Vision and Pattern Recognition*, 2007.
- [34] X.J. Zhou, C.H. Yang, W.H. Gui, A MATLAB toolbox for continuous state transition algorithm, 2016, pp. 9172–9177.
- [35] G.W. Wang, C.H. Yang, H.Q. Zhu, Y.G. Li, X.W. Peng, W.H. Gui, State-transition-algorithm-based resolution for overlapping linear sweep voltammetric peaks with high signal ratio, *Chemom. Intell. Lab. Syst.* 151 (2016) 61–70.
- [36] S. García, D. Molina, M. Lozano, F. Herrera, A study on the use of non-parametric tests for analyzing the evolutionary algorithms' behaviour: a case study on the CEC'2005 special session on real parameter optimization, *J.Heuristics*. DOI:10.1007/s10732-008-9080-4(2008).
- [37] Y. Wang, Z.X. Cai, Q.F. Zhang, Differential evolution with composite trial vector generation strategies and control parameters, *IEEE Trans. Evol. Comput.* 15 (1) (2011) 55–66.